

Modeling of skin tissue heating using the generalized dual phase-lag equation

E. MAJCHRZAK, Ł. TURCHAN, J. DZIATKIEWICZ

*Institute of Computational Mechanics and Engineering
Silesian University of Technology
44-100 Gliwice, Konarskiego 18a, Poland
e-mails: ewa.majchrzak@polsl.pl, lukasz.turchan@polsl.pl,
jolanta.dziatkiewicz@polsl.pl*

THIS PAPER CONCERNS THE NUMERICAL MODELING of skin tissue heating. To describe the analyzed process the system of three generalized dual phase-lag equations corresponding to the successive layers of the skin: epidermis, dermis and sub-cutaneous region is applied. On the surfaces between the layers the ideal thermal contact is assumed, on the skin surface the Neumann condition describing the external heating of tissue can be accepted, and on the remaining surfaces the no-flux condition is taken into account. Initial temperature of the tissue and the blood is known. The problem is solved using the explicit scheme of finite difference method. In the final part of the paper the results of computations are shown.

Key words: bioheat transfer, generalized dual phase-lag equation, finite difference method.

Copyright © 2015 by IPPT PAN

1. Introduction

CONTROLLED HEATING OF BIOLOGICAL TISSUE (artificial hyperthermia) or uncontrolled process of heating (burns) can be modeled using different mathematical descriptions of heat transfer in the living organisms. So far, the most commonly used model is the Pennes equation [1–9]. The bioheat transfer Pennes equation has the essential limitation because it cannot be used to simulate the effect of large, widely spaced thermally significant blood vessels.

In recent years, the several papers devoted to the application of dual phase-lag model in the scope of bioheat processes modeling appeared, e.g., [10–16]. In the dual phase-lag equation (DPL) two lag times are taken into account, in particular, the relaxation and thermalization times. These parameters are assumed on the basis of information resulting from the experiments [17–19] but the numerical values given in the literature vary.

Another approach is to treat the tissue as a porous medium divided into two regions: the vascular region (blood vessels) and the extravascular region (tissue) [20–28]. Then, the mathematical model consists of two equations which

describe the tissue temperature and the blood temperature. The acceptance of the certain assumptions leads to the generalized dual phase-lag equation (GDPLE) (tissue sub-domain) [25] in which the coupling factor and the phase-lag times appear. The phase-lag times are expressed in terms of the blood and tissue properties, the interphase convective heat transfer coefficient and the blood perfusion rate [25]. The GDPLE and the formula concerning the dependence between blood and tissue temperatures supplemented by the appropriate boundary initial conditions create the mathematical model of the process considered. The problem of internal tissue heating is analyzed in [27] using this model.

The purpose of this research is to use the GDPLE for the modeling of skin tissue heating. It should be pointed out that in the case of skin tissue, which has a multilayer structure, a description of the heating process is more difficult (in the very limited number of papers concerning the GDPLE applications – e.g., [20] the homogeneous 1D tissue domain is considered). In this paper the axially symmetrical problem is solved. The temperature distribution in the epidermis is described by Fourier equation, because in this layer the blood vessels do not occur and metabolic heat source is equal to zero, while the temperature distribution in the dermis and in the subcutaneous region is described by generalized dual phase-lag equations, wherein the different dimensions of blood vessels in these layers are taken into account. This system of equations is supplemented by the appropriate boundary and the initial conditions. According to the authors' knowledge, the heat transfer processes in heterogeneous domains described by the system of GDPL equations have not been considered so far. The explicit scheme of the finite difference method for multilayered domain is proposed and the stability criteria are formulated. The FDM algorithm constitutes a basis of 'in house' computer program used for performing numerical modeling. In the final part of the paper the results of computations are shown.

2. Generalized dual phase-lag equation

Heat transfer in the living biological tissues is associated with heat conduction in the tissue, the convective heat transfer between blood vessels and tissue and blood perfusion. The tissue can be treated as a porous medium divided into two regions: the vascular region (blood vessels) and the extravascular region (tissue) as shown in Fig. 1 [25]. To describe the temperature field in these sub-domains the two-equation porous model [25, 29] is applied

$$(2.1) \quad \varepsilon \rho_b c_b \frac{\partial T_b}{\partial t} + \varepsilon \rho_b c_b \mathbf{u} \cdot \nabla T_b + (1 - \varepsilon) \rho c \frac{\partial T}{\partial t} \\ = \varepsilon \nabla(\lambda_b \nabla T_b) + (1 - \varepsilon) \nabla(\lambda \nabla T) + \varepsilon Q_b + (1 - \varepsilon) Q$$

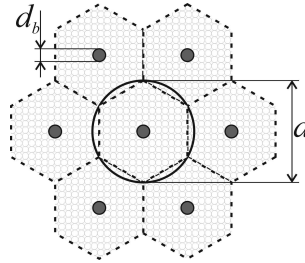


FIG. 1. Assumed tissue structure [25].

and

$$(2.2) \quad \varepsilon \rho_b c_b \frac{\partial T_b}{\partial t} = G(T - T_b),$$

where ε denotes the porosity (the ratio of blood volume to total volume), ρ, ρ_b [kg/m³] are the densities of tissue and blood, respectively, c, c_b [J/(kg · K)] are the specific heats, λ, λ_b [W/(m · K)] are the thermal conductivities, T, T_b [K] are the temperatures, t [s] is the time, Q, Q_b [W/m³] are the metabolic heat sources, \mathbf{u} [m/s] is the blood velocity vector and G [W/(m³ · K)] is the coupling factor.

The coupling factor is defined as [25]

$$(2.3) \quad G = A\alpha + wc_b,$$

where A [m²/m³] is the volumetric heat transfer area between tissue and blood, α [W/(m² · K)] is the heat transfer coefficient and w [kg/(m³ · s)] is the blood perfusion rate.

From Eq. (2.2) the tissue temperature can be determined

$$(2.4) \quad T = T_b + \frac{\varepsilon \rho_b c_b}{G} \frac{\partial T_b}{\partial t}.$$

Introducing the formula (2.4) into Eq. (2.1) one obtains

$$(2.5) \quad \begin{aligned} & \varepsilon \rho_b c_b \frac{\partial T_b}{\partial t} + \varepsilon \rho_b c_b \mathbf{u} \cdot \nabla T_b + (1 - \varepsilon) \rho c \left(\frac{\partial T_b}{\partial t} + \frac{\varepsilon \rho_b c_b}{G} \frac{\partial^2 T_b}{\partial t^2} \right) \\ & = \varepsilon \nabla (\lambda_b \nabla T_b) + (1 - \varepsilon) \nabla \left[\lambda \nabla T_b + \lambda \frac{\varepsilon \rho_b c_b}{G} \frac{\partial (\nabla T_b)}{\partial t} \right] + \varepsilon Q_b + (1 - \varepsilon) Q \end{aligned}$$

or

$$(2.6) \quad \begin{aligned} & C \frac{\partial T_b}{\partial t} + (1 - \varepsilon) \rho c \frac{\varepsilon \rho_b c_b}{G} \frac{\partial^2 T_b}{\partial t^2} + \varepsilon \rho_b c_b \mathbf{u} \cdot \nabla T_b \\ & = \nabla (\Lambda \nabla T_b) + (1 - \varepsilon) \lambda \frac{\varepsilon \rho_b c_b}{G \Lambda} \frac{\partial}{\partial t} [\nabla (\Lambda \nabla T_b)] + \varepsilon Q_b + (1 - \varepsilon) Q, \end{aligned}$$

where

$$(2.7) \quad A = (1 - \varepsilon)\lambda + \varepsilon\lambda_b$$

and

$$(2.8) \quad C = (1 - \varepsilon)\rho c + \varepsilon\rho_b c_b$$

are the effective thermal conductivity and effective heat capacity, respectively.

The phase lags for heat flux and temperature gradient are defined as [25]

$$(2.9) \quad \tau_q = \frac{\varepsilon(1 - \varepsilon)\rho c \rho_b c_b}{GC}$$

and

$$(2.10) \quad \tau_T = \frac{\varepsilon(1 - \varepsilon)\rho_b c_b \lambda}{G\Lambda}$$

As can be observed, the phase-lag times are expressed in terms of the properties of blood and tissue, the interphase convective heat transfer coefficient α and the blood perfusion rate w (cf. Eq. (2.3)). These parameters are closely related to the porosity and, as shown in the paper [25], the greater porosity value determines the greater values of these parameters.

So, Eq. (2.6) can be written as follows:

$$(2.11) \quad C \left(\frac{\partial T_b}{\partial t} + \tau_q \frac{\partial^2 T_b}{\partial t^2} \right) + \varepsilon \rho_b c_b \mathbf{u} \cdot \nabla T_b \\ = \nabla(\Lambda \nabla T_b) + \tau_T \frac{\partial}{\partial t} [\nabla(\Lambda \nabla T_b)] + \varepsilon Q_b + (1 - \varepsilon)Q.$$

It should be pointed out that in Eq. (2.11) the blood temperature and the blood velocity vector are unknown. It is possible, with the additional assumption, to obtain the equation in which the only unknown is the tissue temperature. For this purpose, the blood temperature T_b is determined from Eq. (2.4)

$$(2.12) \quad T_b = T - \frac{\varepsilon \rho_b c_b}{G} \frac{\partial T_b}{\partial t}.$$

Introducing the above dependence to Eq. (2.11) one obtains

$$(2.13) \quad C \left(\frac{\partial T}{\partial t} - \frac{\varepsilon \rho_b c_b}{G} \frac{\partial^2 T_b}{\partial t^2} + \tau_q \frac{\partial^2 T}{\partial t^2} - \tau_q \frac{\varepsilon \rho_b c_b}{G} \frac{\partial^3 T_b}{\partial t^3} \right) \\ + \varepsilon \rho_b c_b \mathbf{u} \cdot \nabla T - \frac{\varepsilon^2 \rho_b^2 c_b^2}{G} \mathbf{u} \cdot \frac{\partial}{\partial t} (\nabla T_b) \\ = \nabla \left[\Lambda \nabla \left(T - \frac{\varepsilon \rho_b c_b}{G} \frac{\partial T_b}{\partial t} \right) \right] \\ + \tau_T \frac{\partial}{\partial t} \left\{ \nabla \left[\Lambda \nabla \left(T - \frac{\varepsilon \rho_b c_b}{G} \frac{\partial T_b}{\partial t} \right) \right] \right\} + \varepsilon Q_b + (1 - \varepsilon)Q$$

or

$$(2.14) \quad C \left(\frac{\partial T}{\partial t} + \tau_q \frac{\partial^2 T}{\partial t^2} \right) \\ = \nabla(\Lambda \nabla T) + \tau_T \frac{\partial}{\partial t} [\nabla(\Lambda \nabla T)] - \varepsilon \rho_b c_b \mathbf{u} \cdot \nabla T \\ + \varepsilon Q_b + (1 - \varepsilon) Q + \frac{\varepsilon \rho_b c_b}{G} \left\{ C \left(\frac{\partial^2 T_b}{\partial t^2} + \tau_q \frac{\partial^3 T_b}{\partial t^3} \right) \right. \\ \left. - \frac{\partial}{\partial t} [\nabla(\Lambda \nabla T_b)] - \tau_T \frac{\partial^2}{\partial t^2} [\nabla(\Lambda \nabla T_b)] + \varepsilon \rho_b c_b \mathbf{u} \cdot \frac{\partial}{\partial t} (\nabla T_b) \right\}.$$

Equation (2.11) is differentiated with respect to time and then

$$(2.15) \quad C \left(\frac{\partial^2 T_b}{\partial t^2} + \tau_q \frac{\partial^3 T_b}{\partial t^3} \right) - \frac{\partial}{\partial t} [\nabla(\Lambda \nabla T_b)] - \tau_T \frac{\partial^2}{\partial t^2} [\nabla(\Lambda \nabla T_b)] \\ + \varepsilon \rho_b c_b \frac{\partial}{\partial t} (\mathbf{u} \cdot \nabla T_b) = \varepsilon \frac{\partial Q_b}{\partial t} + (1 - \varepsilon) \frac{\partial Q}{\partial t}.$$

As can be seen, the left-hand side of Eq. (2.15) is the same as the expression in the curly brackets on the right-hand side of Eq. (2.14). Thus, Eq. (2.14) can be written as

$$(2.16) \quad C \left(\frac{\partial T}{\partial t} + \tau_q \frac{\partial^2 T}{\partial t^2} \right) = \nabla(\Lambda \nabla T) + \tau_T \frac{\partial}{\partial t} [\nabla(\Lambda \nabla T)] \\ - \varepsilon \rho_b c_b \mathbf{u} \cdot \nabla T + \varepsilon Q_b + (1 - \varepsilon) Q + \frac{\varepsilon \rho_b c_b}{G} \left[\varepsilon \frac{\partial Q_b}{\partial t} + (1 - \varepsilon) \frac{\partial Q}{\partial t} \right]$$

or (cf. formula (2.9))

$$(2.17) \quad C \left(\frac{\partial T}{\partial t} + \tau_q \frac{\partial^2 T}{\partial t^2} \right) = \nabla(\Lambda \nabla T) + \tau_T \frac{\partial}{\partial t} [\nabla(\Lambda \nabla T)] \\ - \varepsilon \rho_b c_b \mathbf{u} \cdot \nabla T + \varepsilon Q_b + (1 - \varepsilon) Q + \frac{\tau_q C}{(1 - \varepsilon) \rho c} \left[\varepsilon \frac{\partial Q_b}{\partial t} + (1 - \varepsilon) \frac{\partial Q}{\partial t} \right].$$

If one assumes that [25]

$$(2.18) \quad -\varepsilon \rho_b c_b \mathbf{u} \cdot \nabla T \approx G(T_b - T)$$

then Eq. (2.17) takes the form

$$(2.19) \quad C \left(\frac{\partial T}{\partial t} + \tau_q \frac{\partial^2 T}{\partial t^2} \right) = \nabla(\Lambda \nabla T) + \tau_T \frac{\partial}{\partial t} [\nabla(\Lambda \nabla T)] \\ + G(T_b - T) + \varepsilon Q_b + (1 - \varepsilon) Q + \frac{\tau_q C}{(1 - \varepsilon) \rho c} \left[\varepsilon \frac{\partial Q_b}{\partial t} + (1 - \varepsilon) \frac{\partial Q}{\partial t} \right].$$

It should be pointed out that from the numerical point of view the determination of tissue temperature from Eq. (2.19) and the blood temperature from Eq. (2.12) is very convenient because it does not require the knowledge of velocity vector \mathbf{u} . Taking into account the approximation (2.18), a certain simplification of the model (2.17) is introduced, of course.

To estimate the porosity ε it is assumed that the vessels with diameters d_b are uniformly distributed in the tissue and the entire cross-section area can be considered as a set of recurrent hexagons as shown in Fig. 1 [25]. The diameters of the circles which are equivalent to hexagons are equal to d . So, the porosity can be determined as follows:

$$(2.20) \quad \varepsilon = \frac{d_b^2}{d^2}.$$

To determine the coupling factor it is necessary to know the heat transfer coefficient and the heat transfer area between the tissue and blood (cf. Eq. (2.3)). The heat transfer coefficient can be calculated from the Nusselt number

$$(2.21) \quad \text{Nu} = \frac{\alpha d_b}{\lambda_b} \quad \rightarrow \quad \alpha = \frac{\text{Nu} \lambda_b}{d_b}.$$

To calculate the heat transfer area, the bundle of k blood vessels located in the volume V should be considered. Then, the parameter A has the following form:

$$(2.22) \quad A = \frac{kP_b}{V} = \frac{\varepsilon k P_b}{k V_b} = \frac{\varepsilon \pi d_b L}{\pi (d_b/2)^2 L} = \frac{4\varepsilon}{d_b},$$

where P_b is the surface area between the vessels and tissue, V_b is the volume of blood and L is the length of blood vessels.

In the presented model the blood velocity does not appear explicitly. Parameter describing the blood flow is the blood perfusion rate w [$\text{kg}/(\text{m}^3\text{s})$], as in the Pennes model [1]

$$(2.23) \quad \rho c \frac{\partial T}{\partial t} = \nabla(\lambda \nabla T) + w c_b (T_B - T) + Q,$$

where T_B is the arterial blood temperature. Pennes assumed that the arterial blood temperature T_B is uniform throughout the tissue, while the vein temperature is equal to the tissue temperature at the same point.

For example, in the paper [23] the value of blood flow rate [m^3/s] has been found on the basis of a simple energy balance concerning the steady state problem. The blood temperature change in the relevant sector of the vessel is assumed to be known and then blood flow rate can be obtained. Next, the obtained value is recalculated into the blood velocity v [m/s] in the axial direction.

To summarize, two-temperature model (2.19) and (2.2) supplemented by appropriate boundary and initial conditions allows one to determine the tissue and blood temperatures. In addition, the phase-lag times are expressed in terms of the properties of blood and tissue and the coupling factor between blood and tissue. In this way the non-homogeneous structure of living tissues is taken into account.

3. Formulation of the problem

The domain of skin tissue can be treated as the composition of layers corresponding to the epidermis, dermis and subcutaneous region as shown in Fig. 2.

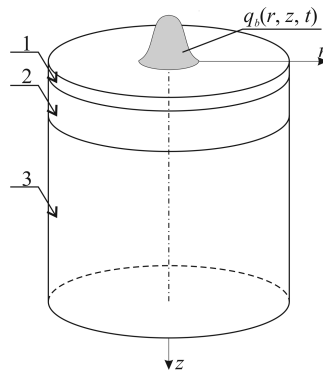


FIG. 2. Axisymmetric fragment of skin tissue (1 – epidermis, 2 – dermis, 3 – sub-cutaneous region).

Because the blood vessels are absent in the epidermis layer, the temperature distribution $T_1 = T_1(r, z, t)$ is described by the following equation:

$$(3.1) \quad C_1 \frac{\partial T_1}{\partial t} = \nabla(\lambda_1 \nabla T_1),$$

where λ_1 is the thermal conductivity of epidermis and $C_1 = c_1 \rho_1$ is the volumetric specific heat of epidermis (c_1 is the specific heat, ρ_1 is the density).

Heat transfer in dermis and subcutaneous region is associated not only with the heat conduction but also with the convective heat transfer between blood vessels and tissue as well as with blood perfusion. So, in each of these layers the tissue can be treated as a porous medium and the temperature distribution in dermis ($e = 2$) and subcutaneous region ($e = 3$) can be described by generalized dual phase-lag equations (here the constant metabolic source functions Q and

Q_b are taken into account – cf. Eq. (2.19)

$$(3.2) \quad C_e \left(\frac{\partial T_e}{\partial t} + \tau_{qe} \frac{\partial^2 T_e}{\partial t^2} \right) \\ = \nabla(\Lambda_e \nabla T_e) + \tau_{T_e} \frac{\partial}{\partial t} [\nabla(\Lambda_e \nabla T_e)] + G_e(T_{be} - T_e) + (1 - \varepsilon_e)Q_e + \varepsilon_e Q_{be},$$

where

$$(3.3) \quad \nabla(\Lambda_e \nabla T_e) = \frac{\partial}{\partial z} \left(\Lambda_e \frac{\partial T_e}{\partial z} \right) + \frac{1}{r} \frac{\partial}{\partial r} \left(r \Lambda_e \frac{\partial T_e}{\partial r} \right),$$

while the blood temperatures in these sub-domains are calculated from the formula (cf. Eq. (2.2))

$$(3.4) \quad T_{be} = T_e - \frac{\varepsilon_e \rho_b c_b}{G_e} \frac{\partial T_{be}}{\partial t}.$$

Equations (3.1), (3.2) and (3.4) should be supplemented by appropriate boundary and initial conditions. So, on the contact surfaces between the layers the ideal thermal contact is assumed, namely

$$(3.5) \quad (r, z) \in \Gamma_1 : \quad \begin{cases} T_1(r, z, t) = T_2(r, z, t), \\ q_1(r, z, t) = q_2(r, z, t), \end{cases}$$

and

$$(3.6) \quad (r, z) \in \Gamma_2 : \quad \begin{cases} T_2(r, z, t) = T_3(r, z, t), \\ q_2(r, z, t) = q_3(r, z, t), \end{cases}$$

where $q_1(r, z, t) = -\lambda_1 \mathbf{n} \cdot \nabla T_1(r, z, t)$, $q_e(r, z, t) = -\Lambda_e \mathbf{n} \cdot \nabla T_e(r, z, t)$, $e = 2, 3$. On the fragment of skin surface: $r \leq r_D$, $z = 0$, for $t \leq t_e$, where t_e is the exposure time, the Neumann condition is proposed [5]

$$(3.7) \quad q_b(r, 0, t) = q_0 \frac{t}{t_e} \left(1 - \frac{t}{t_e} \right) \exp\left(-\frac{r^2}{r_D^2}\right),$$

where q_0 is the constant value. For $t > t_e$: $q_b(r, 0, t) = 0$. On the remaining surfaces of the domain, the no-flux condition is assumed. The initial conditions are also given:

$$(3.8) \quad t = 0 : \quad T_1(r, z, t) = T_p, \quad T_e(r, z, t) = T_p, \quad \frac{\partial T_e(r, z, t)}{\partial t} = 0, \quad e = 2, 3,$$

where T_p is the initial temperature of tissue.

The formulas (3.4) describing the changes of blood temperature are supplemented by the following initial conditions:

$$(3.9) \quad t = 0 : \quad T_{be}(r, z, 0) = T_p, \quad e = 2, 3.$$

4. Method of solution

The formulated problem has been solved using the explicit scheme of finite difference method. The following time grid is introduced:

$$(4.1) \quad 0 = t^0 < t^1 < \dots < t^{f-1} < t^f < \dots < t^F < \infty.$$

The temperature for time $t^f = f\Delta t$ ($f \geq 2$) is denoted as $T^f = T(r, z, f\Delta t)$, where Δt is the constant time step. The uniform spatial grid of dimensions $n \times m$ is shown in Fig. 3.

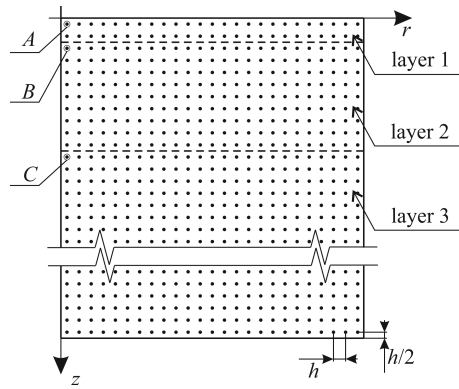


FIG. 3. Spatial discretization.

It is assumed that h is a constant grid step, the same in both directions. It should be noted that the boundary nodes are not located on the boundary of the domain but are shifted by half the grid step (cf. Fig. 3). Then, for node (i, j) the temperature is denoted as $T_{e i, j}^f = (ih - h/2, jh - h/2, f\Delta t)$, where e is the number of particular layers, $i = 1, 2, \dots, n$ and $j = 1, 2, \dots, m$.

The approximation of Eq. (3.4) is as follows:

$$(4.2) \quad T_{be i, j}^f = T_{e i, j}^{f-1} - \frac{\varepsilon_e \rho_b c_b}{G_e} \frac{T_{be i, j}^f - T_{be i, j}^{f-1}}{\Delta t},$$

hence

$$(4.3) \quad T_{be i, j}^f = \frac{G_e \Delta t}{G_e \Delta t + \varepsilon_e \rho_b c_b} \left(T_{e i, j}^{f-1} + \frac{\varepsilon_e \rho_b c_b}{G_e \Delta t} T_{be i, j}^{f-1} \right).$$

As can be seen, when $\varepsilon_1 = 0$, $\tau_{q1} = 0$, $\tau_{T1} = 0$, $G_1 = 0$, $Q_1 = 0$ and $Q_{m1} = 0$ then Eq. (3.2) is the same as Eq. (3.1) describing the temperature distribution in the epidermis. In other words, Eq. (3.2) can be used to determine the temperature in all the layers $e = 1, 2, 3$.

The following approximate form of equations (3.2) is proposed:

$$(4.4) \quad C_e \frac{T_{e,i,j}^f - T_{e,i,j}^{f-1}}{\Delta t} + C_e \tau_{qe} \frac{T_{e,i,j}^f - 2T_{e,i,j}^{f-1} + T_{e,i,j}^{f-2}}{(\Delta t)^2} \\ = \nabla(\Lambda_e \nabla T_e)_{i,j}^{f-1} + \frac{\tau_{Te}}{\Delta t} [\nabla(\Lambda_e \nabla T_e)_{i,j}^{f-1} - \nabla(\Lambda_e \nabla T_e)_{i,j}^{f-2}] \\ + G_e (T_{be,i,j}^f - T_{e,i,j}^{f-1}) + (1 - \varepsilon_e) Q_e + \varepsilon_e Q_{be}$$

or

$$(4.5) \quad C_e \frac{T_{e,i,j}^f - T_{e,i,j}^{f-1}}{\Delta t} + C_e \tau_{qe} \frac{T_{e,i,j}^f - 2T_{e,i,j}^{f-1} + T_{e,i,j}^{f-2}}{(\Delta t)^2} \\ = \frac{\Delta t + \tau_{Te}}{\Delta t} \nabla(\Lambda_e \nabla T_e)_{i,j}^{f-1} \\ - \frac{\tau_{Te}}{\Delta t} \nabla(\Lambda_e \nabla T_e)_{i,j}^{f-2} + G_e (T_{be,i,j}^f - T_{e,i,j}^{f-1}) + (1 - \varepsilon_e) Q_e + \varepsilon_e Q_{be},$$

where (cf. formula (3.3))

$$(4.6) \quad \nabla(\Lambda_e \nabla T_e)_{i,j}^s = \frac{1}{h} \left[\Lambda_{e,i+0.5,j}^s \left(\frac{\partial T_e}{\partial z} \right)_{i+0.5,j}^s - \Lambda_{e,i-0.5,j}^{f-1} \left(\frac{\partial T_e}{\partial z} \right)_{i-0.5,j}^s \right] \\ + \frac{1}{hr_{i,j}} \left[\Lambda_{e,i,j+0.5}^s \left(r \frac{\partial T_e}{\partial r} \right)_{i,j+0.5}^s - \Lambda_{e,i,j-0.5}^s \left(r \frac{\partial T_e}{\partial r} \right)_{i,j-0.5}^s \right]$$

or

$$(4.7) \quad \nabla(\Lambda_e \nabla T_e)_{i,j}^s = \frac{1}{h} \left[\Lambda_{e,i+0.5,j}^s \frac{T_{e,i+1,j}^s - T_{e,i,j}^s}{h} - \Lambda_{e,i-0.5,j}^{f-1} \frac{T_{e,i,j}^s - T_{e,i-1,j}^s}{h} \right] \\ + \frac{1}{hr_{i,j}} \left[\left(r_{i,j} + \frac{h}{2} \right) \Lambda_{e,i,j+0.5}^s \frac{T_{e,i,j+1}^s - T_{e,i,j}^s}{h} - \left(r_{i,j} - \frac{h}{2} \right) \Lambda_{e,i,j-0.5}^s \frac{T_{e,i,j}^s - T_{e,i,j-1}^s}{h} \right],$$

while $s = f - 1$ or $s = f - 2$. The location of intermediate nodes is shown in Fig. 4.

The thermal conductivities in the intermediate nodes are assumed to be the harmonic means of nodal thermal conductivities [30–32], namely

$$(4.8) \quad \Lambda_{e,i-0.5,j}^s = \frac{2\Lambda_{e,i,j}^s \Lambda_{e,i-1,j}^s}{\Lambda_{e,i,j}^s + \Lambda_{e,i-1,j}^s}, \quad \Lambda_{e,i+0.5,j}^{f-1} = \frac{2\Lambda_{e,i,j}^s \Lambda_{e,i+1,j}^s}{\Lambda_{e,i,j}^s + \Lambda_{e,i+1,j}^s}, \\ \Lambda_{e,i,j-0.5}^s = \frac{2\Lambda_{e,i,j}^s \Lambda_{e,i,j-1}^s}{\Lambda_{e,i,j}^s + \Lambda_{e,i,j-1}^s}, \quad \Lambda_{e,i,j+0.5}^s = \frac{2\Lambda_{e,i,j}^s \Lambda_{e,i,j+1}^s}{\Lambda_{e,i,j}^s + \Lambda_{e,i,j+1}^s}.$$

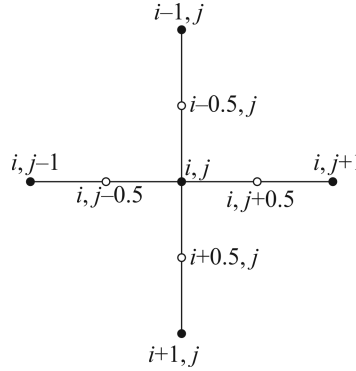


FIG. 4. Five-point star.

Introducing (4.8) into formula (4.7) and after some mathematical reductions, the following form of operator ∇ is obtained:

$$(4.9) \quad \nabla(\Lambda_e \nabla T_e)_{i,j}^s = \Phi_1 \frac{T_{e i,j-1}^s - T_{e i,j}^s}{R_{e i,j1}^s} + \Phi_2 \frac{T_{e i,j+1}^s - T_{e i,j}^s}{R_{e i,j2}^s} + \Phi_3 \frac{T_{e i-1,j}^s - T_{e i,j}^s}{R_{e i,j3}^s} + \Phi_4 \frac{T_{e i+1,j}^s - T_{e i,j}^s}{R_{e i,j4}^s},$$

where

$$(4.10) \quad R_{e i,j1}^s = \frac{h}{2} \left(\frac{1}{\Lambda_{e i,j}^s} + \frac{1}{\Lambda_{e i,j-1}^s} \right), \quad R_{e i,j2}^s = \frac{h}{2} \left(\frac{1}{\Lambda_{e i,j}^s} + \frac{1}{\Lambda_{e i,j+1}^s} \right),$$

$$R_{e i,j3}^s = \frac{h}{2} \left(\frac{1}{\Lambda_{e i,j}^s} + \frac{1}{\Lambda_{e i-1,j}^s} \right), \quad R_{e i,j4}^s = \frac{h}{2} \left(\frac{1}{\Lambda_{e i,j}^s} + \frac{1}{\Lambda_{e i+1,j}^s} \right),$$

$$(4.11) \quad \Phi_1 = \frac{r_{i,j} - 0.5h}{hr_{i,j}}, \quad \Phi_2 = \frac{r_{i,j} + 0.5h}{hr_{i,j}}, \quad \Phi_3 = \Phi_4 = \frac{1}{h}.$$

Summing up, from Eq. (4.5) the temperatures $T_{e i,j}^f$ at all internal nodes i, j are calculated. In the nodes located near the boundary the FDM equations are a little different. For example, for $i = 1$ the boundary condition (3.7) should be taken into account, namely

$$(4.12) \quad r \leq r_D, z = 0 : \quad q_1(r, z, t) = -\lambda_1 \mathbf{n} \cdot \nabla T_1(r, z, t) = q_b(r, z, t);$$

this means

$$(4.13) \quad -\lambda_1 \left(\frac{\partial T}{\partial z} \right)_{i-0.5,j}^s = q_b^s_{i-0.5,j}.$$

The dependence (4.13) is introduced to the formula (4.6) and then ($e = 1$ and $i = 1$):

$$(4.14) \quad \nabla(\lambda_1 \nabla T_1)_{i,j}^s = \frac{1}{h} \left[\lambda_{1^{s_{i+0.5,j}}}^s \left(\frac{\partial T_1}{\partial z} \right)_{i+0.5,j}^s + q_{b^{s_{i-0.5,j}}}^s \right] \\ + \frac{1}{hr_{i,j}} \left[r_{i,j+0.5} \lambda_{1^{s_{i,j+0.5}}}^s \left(\frac{\partial T_e}{\partial r} \right)_{i,j+0.5}^s - r_{i,j-0.5} \lambda_{1^{s_{i,j-0.5}}}^s \left(\frac{\partial T_1}{\partial r} \right)_{i,j-0.5}^s \right].$$

Hence,

$$(4.15) \quad \nabla(\lambda_1 \nabla T_1)_{i,j}^s = \Phi_1 \frac{T_{1^{s_{i,j-1}}}^s - T_{1^{s_{i,j}}}^s}{R_{1^{s_{i,j1}}}^s} + \Phi_2 \frac{T_{1^{s_{i,j+1}}}^s - T_{1^{s_{i,j}}}^s}{R_{e^{s_{i,j2}}}^s} \\ + \Phi_3 q_{b^{s_{i-0.5,j}}}^s + \Phi_4 \frac{T_{1^{s_{i+1,j}}}^s - T_{1^{s_{i,j}}}^s}{R_{1^{s_{i,j4}}}^s}.$$

In the case of explicit scheme of finite difference method application, the stability criterion should be fulfilled, of course. As it is known, solving parabolic equations, two-level difference approximation of time derivative is used and the explicit scheme is stable, if the appropriate coefficients in the FDM equations are non-negative [33]. Here, the hyperbolic equation containing a second-order time derivative and higher-order mixed derivative in both time and space is solved and the problem of stability is more complicated.

To formulate the stability criteria, Eq. (4.5) can be written as follows:

$$(4.16) \quad T_{e^{i,j}}^f = \frac{\Delta t(\Delta t + \tau_{Te})}{C_e(\Delta t + \tau_{qe})} \nabla(\Lambda_e \nabla T_e)_{i,j}^{f-1} - \frac{\tau_{Te} \Delta t}{C_e(\Delta t + \tau_{qe})} \nabla(\Lambda_e \nabla T_e)_{i,j}^{f-2} \\ + \frac{\Delta t + 2\tau_{qe}}{\Delta t + \tau_{qe}} T_{e^{i,j}}^{f-1} - \frac{\tau_{qe}}{\Delta t + \tau_{qe}} T_{e^{i,j}}^{f-2} + \frac{G_e(\Delta t)^2}{C_e(\Delta t + \tau_{qe})} (T_{be^{i,j}}^f - T_{e^{i,j}}^{f-1}) \\ + \frac{(\Delta t)^2}{C_e(\Delta t + \tau_{qe})} [(1 - \varepsilon_e) Q_e + \varepsilon_e Q_{be}]$$

or using the dependence (4.9)

$$(4.17) \quad T_{e^{i,j}}^f = \left[\frac{\Delta t + 2\tau_{qe}}{\Delta t + \tau_{qe}} - \frac{\Delta t(\Delta t + \tau_{Te})}{C_e(\Delta t + \tau_{qe})} \left(\frac{\Phi_1}{R_{e^{i,j1}}^{f-1}} + \frac{\Phi_2}{R_{e^{i,j2}}^{f-1}} + \frac{\Phi_3}{R_{e^{i,j3}}^{f-1}} + \frac{\Phi_4}{R_{e^{i,j4}}^{f-1}} \right) - \frac{G_e(\Delta t)^2}{C_e(\Delta t + \tau_{qe})} \right] T_{e^{i,j}}^{f-1} \\ + \frac{\Delta t(\Delta t + \tau_{Te})}{C_e(\Delta t + \tau_{qe})} \left(\frac{\Phi_1}{R_{e^{i,j1}}^{f-1}} T_{e^{i,j-1}}^{f-1} + \frac{\Phi_2}{R_{e^{i,j2}}^{f-1}} T_{e^{i,j+1}}^{f-1} + \frac{\Phi_3}{R_{e^{i,j3}}^{f-1}} T_{e^{i-1,j}}^{f-1} + \frac{\Phi_4}{R_{e^{i,j4}}^{f-1}} T_{e^{i+1,j}}^{f-1} \right) \\ - \left[\frac{\tau_{qe}}{\Delta t + \tau_{qe}} - \frac{\tau_{Te} \Delta t}{C_e(\Delta t + \tau_{qe})} \left(\frac{\Phi_1}{R_{e^{i,j1}}^{f-2}} + \frac{\Phi_2}{R_{e^{i,j2}}^{f-2}} + \frac{\Phi_3}{R_{e^{i,j3}}^{f-2}} + \frac{\Phi_4}{R_{e^{i,j4}}^{f-2}} \right) \right] T_{e^{i,j}}^{f-2}$$

$$\begin{aligned}
 & -\frac{\tau_{Te}\Delta t}{C_e(\Delta t + \tau_{qe})} \left(\frac{\Phi_1}{R_{e i, j1}^{f-2}} T_{e i, j-1}^{f-2} + \frac{\Phi_2}{R_{e i, j2}^{f-2}} T_{e i, j+1}^{f-2} + \frac{\Phi_3}{R_{e i, j3}^{f-2}} T_{e i-1, j}^{f-2} + \frac{\Phi_4}{R_{e i, j4}^{f-2}} T_{e i+1, j}^{f-2} \right) \\
 & + \frac{G_e(\Delta t)^2}{C_e(\Delta t + \tau_{qe})} T_{be i, j}^f + \frac{(\Delta t)^2}{C_e(\Delta t + \tau_{qe})} [(1 - \varepsilon_e)Q_e + \varepsilon_e Q_{be}].
 \end{aligned}$$

Equation (4.17) is a three-level difference approximation, and the condition similar as in the case of two-level scheme must be fulfilled

$$\begin{aligned}
 (4.18) \quad & \frac{\Delta t + 2\tau_{qe}}{\Delta t + \tau_{qe}} - \frac{\Delta t(\Delta t + \tau_{Te})}{C_e(\Delta t + \tau_{qe})} \left(\frac{\Phi_1}{R_{e i, j1}^{f-1}} + \frac{\Phi_2}{R_{e i, j2}^{f-1}} + \frac{\Phi_3}{R_{e i, j3}^{f-1}} + \frac{\Phi_4}{R_{e i, j4}^{f-1}} \right) \\
 & - \frac{G_e(\Delta t)^2}{C_e(\Delta t + \tau_{qe})} \geq 0.
 \end{aligned}$$

The authors performed numerous computations with a wide range of values of h and Δt which suggest that the condition (4.18) is not sufficient and the unconditional stability appears when additionally appropriate coefficients in the difference equations (4.17) occurring at temperatures for the time t^{f-2} are negative. Thus,

$$(4.19) \quad \frac{\tau_{qe}}{\Delta t + \tau_{qe}} - \frac{\tau_{Te}\Delta t}{C_e(\Delta t + \tau_{qe})} \left(\frac{\Phi_1}{R_{e i, j1}^{f-2}} + \frac{\Phi_2}{R_{e i, j2}^{f-2}} + \frac{\Phi_3}{R_{e i, j3}^{f-2}} + \frac{\Phi_4}{R_{e i, j4}^{f-2}} \right) \geq 0,$$

but it is not proven mathematically. Summing up, in the case of the proposed algorithm both of the conditions (4.18) and (4.19) must be fulfilled. This is also confirmed by the results presented in [34]. So, it is necessary to choose such a time step Δt and a grid step h for which these inequalities are satisfied. In this paper, for the assumed grid step h and for each skin layer e , $e = 1, 2, 3$, the time steps $\Delta t_1, \Delta t_2, \Delta t_3$ were chosen in order to fulfil these stability criteria and next in the calculations the time step $\Delta t = \min\{\Delta t_1, \Delta t_2, \Delta t_3\}$ is accepted.

5. Results of computations

The domain of skin tissue (cylinder of dimensions $R = Z = 0.0121$ m) shown in Fig. 2 is considered. The thicknesses of successive layers of skin are equal to $z_1 = 0.0001$ m, $z_2 = 0.002$ m and $z_3 = 0.01$ m, respectively. The initial temperature of tissue and blood is equal to $T_p = 37^\circ\text{C}$. In Table 1 the thermophysical parameters of all tissue layers and the blood are collected [2].

Calculations are performed for $r_D = R/4$, $q_0 = 20$ kW/m² and $t_e = 100$ s (cf. formula (3.7)). In Fig. 5 the course of boundary heat flux for selected times is presented.

Table 1. Thermophysical parameters of tissue layers and blood [2].

	Layer 1	Layer 2	Layer 3	Blood
Density [kg/m^3]	$\rho_1 = 1200$	$\rho_2 = 1200$	$\rho_3 = 1000$	$\rho_b = 1060$
Specific heat [$\text{J}/(\text{kg} \cdot \text{K})$]	$c_1 = 3589$	$c_2 = 3300$	$c_3 = 2674$	$c_b = 3770$
Thermal conductivity [$\text{W}/(\text{m} \cdot \text{K})$]	$\lambda_1 = 0.235$	$\lambda_2 = 0.445$	$\lambda_3 = 0.185$	$\lambda_b = 0.5$
Metabolic heat source [W/m^3]	$Q_{m1} = 0$	$Q_{m2} = 245$	$Q_{m3} = 245$	$Q_{mb} = 245$

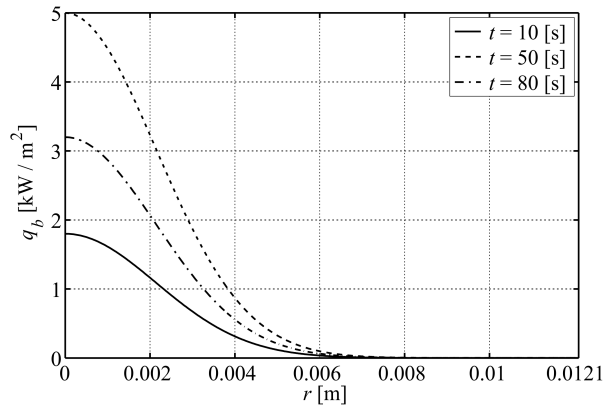


FIG. 5. Distribution of boundary heat flux along the radius of the cylinder.

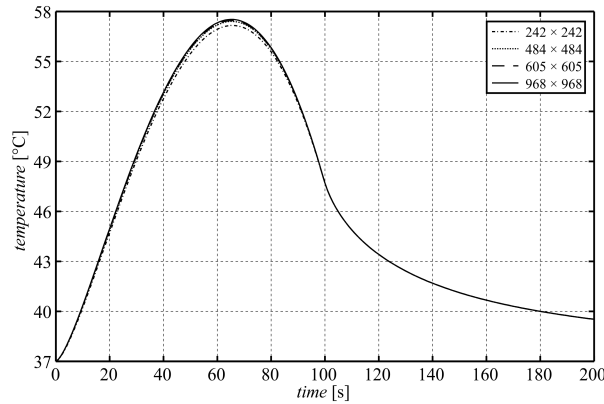


FIG. 6. Time history of tissue temperature at point A for different number of grid nodes.

The parameters necessary to determine the porosity and coupling factors for second and third layers of skin are also taken from the literature [25] and summarized along with the calculated data in Table 2. The Nusselt number is assumed as $\text{Nu} = 4.93$ [35].

Table 2. Parameters of the blood supplied layers.

	Layer 2	Layer 3
Vessel diameter [m]	$d_{b2} = 0.00114$	$d_{b3} = 0.00228$
Diameter of circles equivalent to hexagons [m]	$d_2 = 0.01783$	$d_3 = 0.01982$
Porosity	$\varepsilon_2 = 0.0041$	$\varepsilon_3 = 0.0132$
Perfusion rate [$\text{kg}/(\text{m}^3 \cdot \text{s})$]	$w_2 = 1$	$w_3 = 1$
Coupling factor [$\text{W}/(\text{m}^3 \cdot \text{K})$]	$G_2 = 34785.174$	$G_3 = 28869.763$
Relaxation time [s]	$\tau_{q2} = 0.46772$	$\tau_{q3} = 1.80753$
Thermalization time [s]	$\tau_{T2} = 0.46771$	$\tau_{T3} = 1.80751$
Effective thermal conductivity [$\text{W}/(\text{m} \cdot \text{K})$]	$\Lambda_2 = 0.4452$	$\Lambda_3 = 0.1892$
Effective volumetric heat capacity [$\text{MJ}/(\text{m}^3 \cdot \text{K})$]	$C_2 = 3.9601$	$C_3 = 2.6915$
Blood velocity [m/s] [23]	$v_2 = 12.29$	$v_3 = 3.8$

As was mentioned earlier, the problem is solved by means of the finite difference method. It should be pointed out that in order to check whether the results are grid independent, the calculations were done for 242×242 , 484×484 , 605×605 and 968×968 nodes (Fig. 6) under the assumption that the time step is equal to $\Delta t = 0.0001$ s. In further calculations the differential grid with 605×605 nodes is used and the time step is equal to $\Delta t = 0.0005$ s.

History of tissue temperature at points A ($10^{-5}; 10^{-5}$), B ($10^{-5}; 1.1 \cdot 10^{-4}$) and C ($10^{-5}; 2.11 \cdot 10^{-3}$) (all coordinates are given in meters) marked in Fig. 3 is shown in Fig. 7. At point A maximum temperature 57.08°C occurs after 65 s and at point B maximum temperature 57.29°C occurs after 67 s. At point C the maximum temperature occurs after 86 s and is equal to 45.43°C . As can be seen

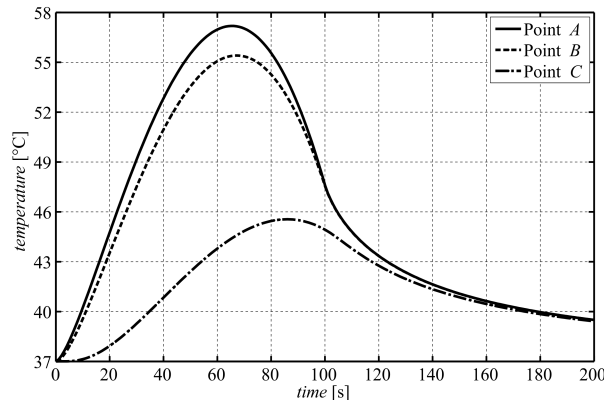


FIG. 7. Time history of tissue temperature at selected points.

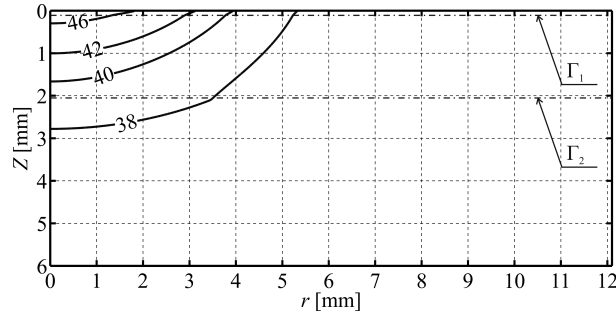


FIG. 8. Distribution of tissue temperature after 30 seconds.

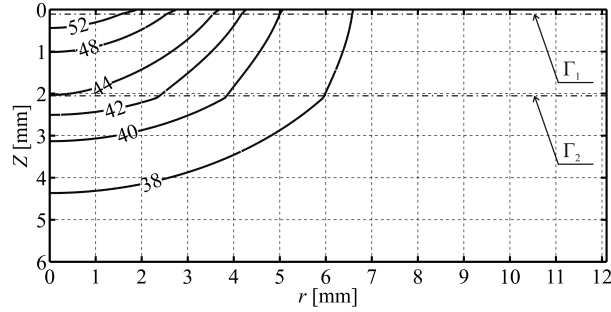


FIG. 9. Distribution of tissue temperature after 60 seconds.

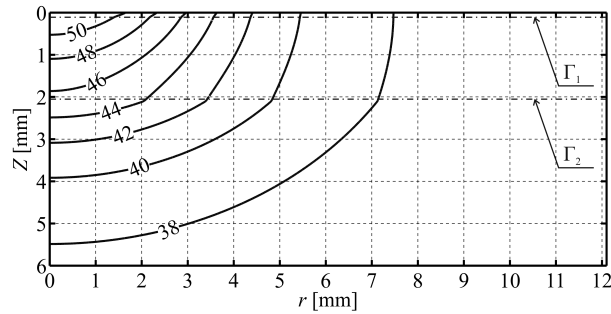


FIG. 10. Distribution of tissue temperature after 90 seconds.

in Fig. 7, after 180 s the tissue temperature at points A , B and C is almost the same.

In Figs. 8, 9 and 10 the distribution of tissue temperature in the part of the domain ($z \leq 0.006$ m) is presented. The boundaries between the layers are marked as Γ_1 and Γ_2 , respectively.

In Figure 11 the courses of tissue and blood temperature at point C marked in Fig. 3 are shown. It is visible, that these temperatures are very similar.

As was mentioned before, the numerical modeling of skin tissue heating on the basis of the system of Pennes equations can be also used [2, 5, 7, 8]. If in Eqs. (3.2) one assumes that $\varepsilon_e = 0$ (in this case $C_e = \rho_e c_e$, $\Lambda_e = \lambda_e$, $\tau_{qe} = 0$, $\tau_{Te} = 0$), $G_e = wc_b$ and $T_{be} = T_B$, where $T_B = 37^\circ\text{C}$ is the arterial blood temperature, then these equations are reduced to the Pennes ones (cf. Eq. (2.23)). Thus, the calculations both for the GDPLE and for the Pennes equations can be performed using the same computer program.

Comparison of the results obtained using these models is shown in Fig. 11 (the solution corresponding to the GDPL model has been obtained using the data collected in Table 2). The slight differences are due to the fact that the low porosity values of ε_2 and ε_3 are assumed here. At the same time, this comparison confirms the correctness of the proposed algorithm. For the higher porosity values the differences between the temperatures obtained using both models are significant [36]. To show these differences, the calculations have been repeated under the assumption that the porosity of subcutaneous region is equal to $\varepsilon_3 = 0.1637$ ($d_{b3} = 0.00456$ m, $d_3 = 0.01127$ m, $w_3 = 5$ kg/(m³ · s) [25] and then $G_3 = 96479.910$ W/(m³ · K), $\tau_{q3} = 5.67173$ s, $\tau_{T3} = 5.67085$ s). In Fig. 12 the history of tissue and blood temperatures at point C obtained using the GDPL model and the history of tissue temperature obtained using the Pennes model are shown.

As can be seen, in the case of GDPLE the blood and tissue temperatures differ significantly, and during the heating process they are lower than the temperature obtained from the Pennes equation. Moreover, comparing the results shown in Figs. 11 and 12, it is visible that when the porosity is higher (in this case

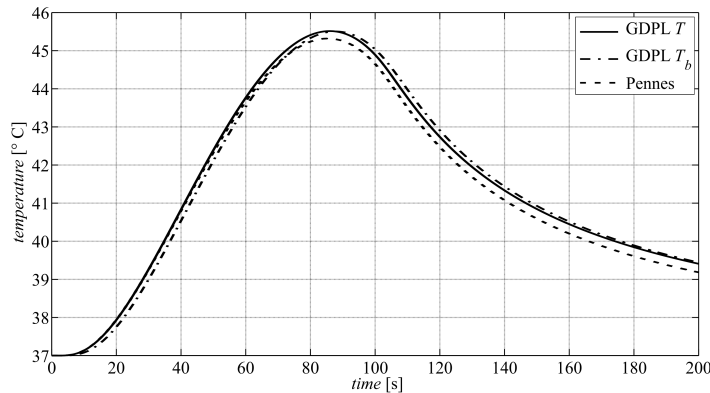


FIG. 11. Time history of tissue and blood temperature at point C and comparison with the Pennes model.

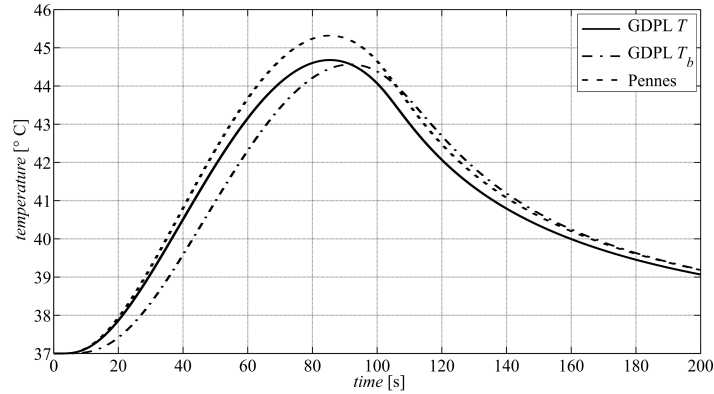


FIG. 12. Time history of tissue and blood temperature at point C and comparison with the Pennes model ($\varepsilon_3 = 0.1637$).

the relaxation time and the thermalization time are also longer) the differences between the temperatures T and T_b are greater.

6. Conclusions

Cylindrical domain of layered structure of skin tissue is considered. To determine the temperature distribution in the heated skin tissue the system of generalized dual phase-lag equations is used, while the blood temperature in dermis and subcutaneous regions is calculated on the basis of formulas describing the relationships between tissue and blood temperatures. It should be pointed out that the coupling factors and the phase-lag times occurring in the mathematical model contain the information about the properties of the blood, interphase convective heat transfer coefficients and blood perfusion rates.

The problem is solved using the explicit scheme of finite difference method and the results of computations confirm the effectiveness of the presented algorithm.

Temperature distribution of the tissue and blood obtained using the proposed algorithm can be applied, among others, in numerical modeling of laser-biological tissue interactions [10, 11, 39], burn predictions [7, 8] and also for estimation of admissible thermal dose [5, 37, 38] or degree of thermal damage (Arrhenius integral) during the skin tissue heating.

7. Acknowledgements

This paper is a part of the project sponsored by the National Science Centre DEC 2011/01/N/ST6/05231.

References

1. H.H. PENNES, *Analysis of tissue and arterial blood temperatures in the resting human forearm*, Journal of Applied Physiology, **1**, 93–122, 1948.
2. D.A. TORVI, J.D. DALE, *A finite element model of skin subjected to a flash fire*, Journal of Biomechanical Engineering, **116**, 250–255, 1994.
3. M. JAMIL, E.Y.K. NG, *Ranking of parameters in bioheat transfer using Taguchi analysis*, International Journal of Thermal Sciences, **63**, 15–21, 2013.
4. B. MOCHNACKI, E. MAJCHRZAK, *Sensitivity of the skin tissue on the activity of external heat sources*, CMES: Computer Modeling in Engineering and Sciences, **4**, 3–4, 431–438, 2003.
5. B. MOCHNACKI, A. PIASECKA-BELKHAYAT, *Numerical modeling of skin tissue heating using the interval finite difference method*, MCB: Molecular & Cellular Biomechanics, **10**, 3, 233–244, 2013.
6. M. JASIŃSKI, *Investigation of tissue thermal damage process with application of direct sensitivity method*, MCB: Molecular & Cellular Biomechanics, **10**, 3, 183–199, 2013.
7. E. MAJCHRZAK, B. MOCHNACKI, M. DZIEWOŃSKI, M. JASIŃSKI, *Numerical modelling of hyperthermia and hypothermia processes*, Computational Materials Science, **268–270**, 257–262, 2011.
8. E. MAJCHRZAK, B. MOCHNACKI, M. JASIŃSKI, *Numerical modelling of bioheat transfer in multi-layer skin tissue domain subjected to a flash fire*, Computational Fluid and Solid Mechanics, **1–2**, 1766–1770, 2003.
9. A. MALEK, G. ABBASI, *Optimal control solution for Pennes' equation using strongly continuous semigroup*, Kybernetika, **50**, 4, 530–543, 2014.
10. J. ZHOU, J.K. CHEN, Y. ZHANG, *Dual phase lag effects on thermal damage to biological tissues caused by laser irradiation*, Computers in Biology and Medicine, **39**, 286–293, 2009.
11. J. ZHOU, Y. ZHANG, J.K. CHEN, *An axisymmetric dual-phase lag bio-heat model for laser heating of living tissues*, International Journal of Thermal Sciences, **48**, 8, 1477–1485, 2009.
12. KUO-CHI LIU, HAN-TAW CHEN, *Investigation for the dual phase lag behavior of bioheat transfer*, International Journal of Thermal Sciences, **49**, 1138–1146, 2010.
13. E. MAJCHRZAK, *Numerical solution of dual phase lag model of bioheat transfer using the general boundary element method*, CMES: Computer Modeling in Engineering & Sciences, **69**, 1, 43–60, 2010.
14. N. AFRIN, Y. ZHANG, J.K. CHEN, *Thermal lagging in living biological tissue based on non-equilibrium heat transfer in a three-carrier system*, International Journal of Heat and Mass Transfer, **54**, 2419–2426, 2011.
15. A. MALEK, Z.K. BOJDI, P.N.N. GOLBARG, *Solving fully three-dimensional microscale dual phase lag problem using mixed-collocation, finite difference discretization*, Journal of Heat Transfer, **134**, 9, 094501–094506, 2012.
16. E. MAJCHRZAK, Ł. TURCHAN, *The general boundary element method for 3D dual-phase lag model of bioheat transfer*, Engineering Analysis with Boundary Elements, **50**, 76–82, 2015.

17. W. KAMINSKI, *Hyperbolic heat conduction equation for materials with a nonhomogeneous inner structure*, Journal of Heat Transfer, **112**, 555–560, 1990
18. K. MITRA, S. KUMAR, A. VEDAVARZ, M.K. MOALLEMI, *Experimental evidence of hyperbolic heat conduction in processed meat*, Journal of Heat Transfer, **117**, 568–573, 1995.
19. P.J. ANTAKI, *New interpretation of non-Fourier heat conduction in processed meat*, Journal of Heat Transfer, **127**, 189–193, 2005.
20. N. AFRIN, J. ZHOU, Y. ZHANG, D.Y. TZOU, J.K. CHEN, *Numerical simulation of thermal damage to living biological tissues induced by laser irradiation based on a generalized dual phase lag model*, Numerical Heat Transfer, Part A: Applications, **61**, 7, 483–501, 2012.
21. A.R.A. KHALED, K. VAFAI, *The role of porous media in modeling of flow and heat transfer in biological tissues*, International Journal of Heat and Mass Transfer, **46**, 4989–5003, 2003.
22. A. NAKAYAMA, F. KUWAHARA, *A general bioheat transfer model based on the theory of porous media*, International Journal of Heat and Mass Transfer, **51**, 3190–3199, 2008.
23. P. YUAN, *Numerical analysis of an equivalent heat transfer coefficient in a porous model for simulating a biological tissue in a hyperthermia therapy*, International Journal of Heat and Mass Transfer, **52**, 1734–1740, 2009.
24. N. AFRIN, Y. ZHANG, J.K. CHEN, *Thermal lagging in living biological tissue based on nonequilibrium heat transfer between tissue, arterial and venous bloods*, International Journal of Heat and Mass Transfer, **54**, 2419–2426, 2011.
25. Y. ZHANG, *Generalized dual-phase lag bioheat equations based on nonequilibrium heat transfer in living biological tissues*, International Journal of Heat and Mass Transfer, **52**, 4829–4834, 2009.
26. E. MAJCHRZAK, Ł. TURCHAN, *Numerical analysis of tissue heating using the bioheat transfer porous model*, Computer Assisted Methods in Engineering and Science, **20**, 2, 123–131, 2013.
27. E. MAJCHRZAK, Ł. TURCHAN, *A numerical analysis of heating tissue using the two-temperature model*, Advanced Computational Methods and Experiments in Heat Transfer XIII, WIT Transactions on Engineering Sciences, **83**, 477–488, 2014.
28. E. MAJCHRZAK, Ł. TURCHAN, *Numerical analysis of tissue heating using the generalized dual phase lag model*, Recent Advances in Computational Mechanics, Łodygowski, Rakowski & Litewka (eds.), Taylor & Francis Group, London, 355–362, 2014.
29. W.J. MINKOWYCZ, A. HAJI-SHEIKH, K. VAFAI, *On departure from local thermal equilibrium in porous media due to a rapidly changing heat source: the Sparrow number*, International Journal of Heat Mass Transfer, **42**, 18, 3373–3385, 1999.
30. Z. DOMAŃSKI, M. CIESIELSKI, B. MOCHNACKI, *Application of control volume method using the Voronoi tessellation in numerical modelling of solidification process*, Current Themes in Engineering Science 2009, Book Series: AIP Conference Proceedings, **1220**, 17–26, 2010.
31. M. DZIEWOŃSKI, B. MOCHNACKI, R. SZOPA, *Sensitivity of biological tissue freezing process on the changes of cryoprobe cooling rate*, Book Series: Mechanika, Kaunas University of Technology, 82–87, 2011.

-
32. B. MOCHNACKI, M. CIESIELSKI, *Numerical model of thermal processes in domain of thin film subjected to a cyclic external heat flux*, THERMEC 2011, PTS 1-4 Book Series: Materials Science Forum, **706–709**, 1460–1465, 2012.
 33. B. MOCHNACKI, J.S. SUCHY, *Numerical methods in computations of foundry processes*, PFTA, Cracow, 1995.
 34. J.M. McDONOUGH, I. KUNADIAN, R.R. KUMAR, T. YANG, *An alternative discretization and solution procedure for the dual phase-lag equation*, Journal of Computational Physics, **219**, 1, 163–171, 2006.
 35. A.K. COUSINS, *On the Nusselt number in heat transfer between multiple parallel blood vessels*, Journal of Biomechanical Engineering, **119**, 1, 127–129, 1997.
 36. Ł. TURCHAN, *Numerical analysis of artificial hyperthermia using different models of bio-heat transfer*, Doctoral Thesis, Silesian University of Technology, Gliwice, 2014.
 37. S.A. SAPARETO, W.C. DEWEY, *Thermal dose determination in cancer therapy*, International Journal of Radiation Oncology Biology Physics, **10**, 6, 787–800, 1984.
 38. E. MAJCHRZAK, Ł. TURCHAN, *Numerical estimation of thermal dose during hyperthermia treatment using the BEM*, Mechanika 2011: Proceedings of the 16th International Conference, Book Series: Mechanika, Kaunas University of Technology, 215–219, 2011.
 39. W. DAI, H. WANG, P.M. JORDAN, R.E. MICKENS, A. BEJAN, *A mathematical model for skin burn injury induced by radiation heating*, International Journal of Heat and Mass Transfer, **51**, 5497–5510, 2008.

Received August 28, 2014; revised version June 12, 2015.
